Microstructure and Magnetic Studies of Zinc Ferrite Nano-Particles

N. M. Deraz[*]*, A. Alarifi*

Catalytic Chemistry Chair, Chemistry Department , College of Science, King Saud University, P.O. Box 2455, Riyadh 11451, Saudi Arabia

[*]E-mail: nmderaz@yahoo.com

Zinc ferrite nano-particles are synthesised by advanced combustion route. The nano-sized Zn ferrite characterized by X-ray diffraction (XRD), Scanning electron micrographs (SEM) and Energy dispersive X-ray (EDX) techniques. The magnetic properties were determined by using vibrating sample magnetometer (VSM). The preparation method investigated brought about formation of moderate crystalline $ZnFe_2O_4$ as a single phase with irregular shape. Both the saturation magnetization (60 emu/g) and the remnant magnetization (20 emu/g) were found to be highly depending upon the size and crystallinity of the investigated ferrite. Our results indicate that this method might provide a promising option for synthesizing high-quality nano-sized $ZnFe_2O_4$.

1. INTRODUCTION

Ferrite material has been widely used in various technical applications including in magnetic refrigeration, detoxification of biological fluids, magnetically controlled transport of anti-cancer drugs, magnetic resonance imaging contrast enhancement, magnetic cell separation, magnetic devices, switching devices, recording tapes, permanent magnets, hard disc recording media, flexible recording media, read-write heads, active components of ferrofluids, color imaging, gas-sensitive materials and catalytic materials [1-7]. Ferrite based nano-materials show novel properties that are often significantly different from the bulk due to fundamental changes in structural and concomitant electronic rearrangements (induced by the reduced dimensionality) and to significant dominance of the surface atoms. [8–10]. Among the ferrite materials, zinc ferrite that has been many applications in various fields of industry including magnetic materials, gas sensor and absorbent material for hot-gas

desulphurization [11-14]. Recently, it was found that Zn ferrite is a promising semiconductor photo-catalyst for various processes due to its ability to absorb visible light, high efficiency, low cost and excellent photochemical stability. In addition, zinc ferrite shows potentially wide applications in photo induced electron transfer, photo-electrochemical cells and photo-chemical hydrogen production [15-22]. Zinc ferrite is fabricated by numerous methods, such as ceramic method, sol–gel, co-precipitation, ball-milling technique, hydrothermal synthesis and thermal decomposition [23-27].

The traditional bulk $ZnFe_2O_4$ is a normal spinel with Zn^{2+} ions only on the tetrahedral (A) sites and Fe^{3+} ions only on the octahedral (B) sites. It has antiferromagnetic properties below the Néel temperature of about 10 K and behaves paramagnetic at room temperature [28]. Recent investigations of nano-crystalline $ZnFe_2O_4$ have suggested that the cation distribution in this material is partly inverted and exhibits anomaly in its magnetization [28, 29]. Néel suggested that small antiferromagnetic particles can exhibit super-paramagnetism and weak ferromagnetism due to uncompensated spins in the two sublattices [30]. One of the most challenging open questions in the study of spinel ferrite nanoparticles is the cation distribution between the two interstitial sites of the structure and its influence on the different properties of the ferrite materials. Indeed, the cation distribution over the tetrahedral and octahedral sites in the spinel-type lattice is strongly dependent on the ionic radii, concentration of the substituted divalent metal ions and the synthesis pathway [31-34]. Large cation redistributions/inversion parameters can be obtained only by placing $ZnFe_2O_4$ into a non-equilibrium state [35].

In recent years, combustion synthesis of zinc ferrite has attracted the interest of many researchers as an energy and time-saving process [31–34, 36, 37]. In addition, this method resulted in ceramic products have high purity, chemical homogeneity on an atomic scale, small uniform particle sizes and controlled particle shapes. In previous our investigations, the combustion route with different fuels have been used to synthesize undoped and Li, Mg and Al doped zinc ferrites [31-34]. These studies showed that the molar ratio of fuel and doping affect the cation distribution between the two interstitial sites of the spinel structure with subsequent modification in different properties of the as prepared ferrites.

The present work aims to investigate the structural, morphologically and magnetic properties of Zn ferrite sample which prepared by using the advanced combustion method. Detailed analyses of the structural, morphologically and magnetic properties of as prepared ferrite are discussed. The techniques employed were XRD, SEM, EDX and VSM.

2. EXPERIMENTAL

2.1. Materials

Zn/Fe mixed oxide sample was prepared by mixing calculated proportions of zinc and iron nitrates with a mixture of glycine and ammonium nitrate. The mixed precursors were concentrated in a porcelain crucible on a hot plate at 350 $^{\circ}$C for 10 minutes. The crystal water was gradually vaporized during heating and when a crucible temperature was reached, a great deal of foams produced and spark

appeared at one corner which spread through the mass, yielding a brown voluminous and fluffy product in the container. In our experiment, the ratio of the H_4NNO_3: H_2NCH_2COOH: $Zn(NO_3)_2.6H_2O$: $Fe(NO_3)_3.9H_2O$ were 1: 4 : 1 : 2, respectively. The chemicals employed in the present work were of analytical grade supplied by Prolabo Company.

2.2. Techniques

An X-ray measurement of various mixed solids was carried out using a BRUKER D8 advance diffractometer (Germany). The patterns were run with Cu K_α radiation at 40 kV and 40 mA with scanning speed in 2θ of 2 ° min^{-1}.

The crystallite size of Zn-ferrite present in the investigated solids was based on X-ray diffraction line broadening and calculated by using Scherrer equation [38].

$$d = \frac{B\lambda}{\beta \cos\theta} \tag{1}$$

where d is the average crystallite size of the phase under investigation, B is the Scherrer constant (0.89), λ is the wave length of X-ray beam used, β is the full-with half maximum (FWHM) of diffraction and θ is the Bragg's angle.

Scanning electron micrographs (SEM) were recorded on SEM-JEOL JAX-840A electron microanalyzer (Japan). The samples were dispersed in ethanol and then treated ultrasonically in order disperse individual particles over a gold grids.

Energy dispersive X-ray (EDX) analysis was carried out on Hitachi S-800 electron microscope with an attached kevex Delta system. The parameters were as follows: accelerating voltage 10, 15 and 20 kV, accumulation time 100s, window width 8 μm. The surface molar composition was determined by the Asa method, Zaf-correction, Gaussian approximation.

The magnetic properties of the investigated solids were measured at room temperature using a vibrating sample magnetometer (VSM; 9600-1 LDJ, USA) in a maximum applied field of 15 kOe. From the obtained hysteresis loops, the saturation magnetization (M_s), remanence magnetization (M_r) and coercivity (H_c) were determined.

3. RESULTS

3.1. XRD investigation

The XRD pattern of the as synthesized solid is shown in Fig.1. This figure showed that the as prepared sample consisted entirely of nano-crystalline $ZnFe_2O_4$ particles. Indeed, the XRD pattern contains ten sharp lines coincide with the standard data of the cubic spinel Zn ferrite (Franklinite)

phase with the Fd3m space group (JCPDS card No. 74-2397). The peaks of the as prepared solid indexed to the crystal plane of spinel Zn ferrite (220), (311), (222), (400), (422), (511), (440), (620), (533) and (622), respectively. The crystallite size of this ferrite was estimated to be about 52 nm from the X-ray peak broadening of the (311) peak using Scherrer's equation. The X-ray pattern of the as prepared ferrite displays sharp and well-resolved diffraction peaks with the good crystallinity of the as prepared specimen. No additional peak of the second phase was observed in the XRD pattern, showing that the as prepared ferrite consisted of single spinel $ZnFe_2O_4$ phase.
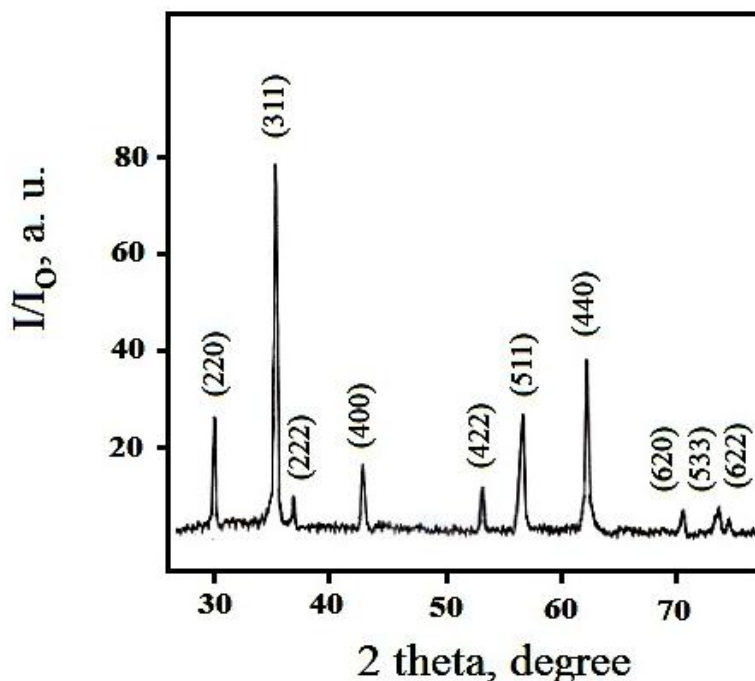

Figure 1. XRD pattern for cubic spinel $ZnFe_2O_4$ nano-particles.

An X-ray data enable us to calculate the different structural parameters such as the lattice constant (a), unit cell volume (V), X-ray density (D_x), the distance between the magnetic ions (L_A and L_B), ionic radii (r_A, r_B) and bond lengths (A–O and B–O) on tetrahedral (A) sites and octahedral (B) sites of cubic spinel structure for the produced zinc ferrite crystallites. The calculated values of a, L_A, L_B , r_A, r_B, A–O and B–O of Mn ferrite are 0.8444, 0.3656, 0.2985, 0.0552, 0.0719, 0.1902 and 0.2069 nm, respectively. Whereas, the value of V is 0.602 nm^3 while the value of D_x is 5.3207 g/cm^3.

3.2. SEM measurement

SEM micrographs of as-prepared powders with different magnifications are shown in Fig. 2a-d. This figure displays the formation of spongy and fragile zinc ferrite powders. The fracture surfaces of the aggregated powders are formed by using a mixture of glycine with ammonium nitrate. In addition, the as synthesized sample consisted of multigrain agglomerations with small discrete crystallites. One

can see voids and pores in the samples. This observation could be attributed to the release of large amount gases during combustion process due decomposition of both glycine and ammonium nitrate. By comparing with my previous work, it is found that the zinc ferrite prepared by using a mixture of glycine and ammonium nitrate displays week agglomeration.
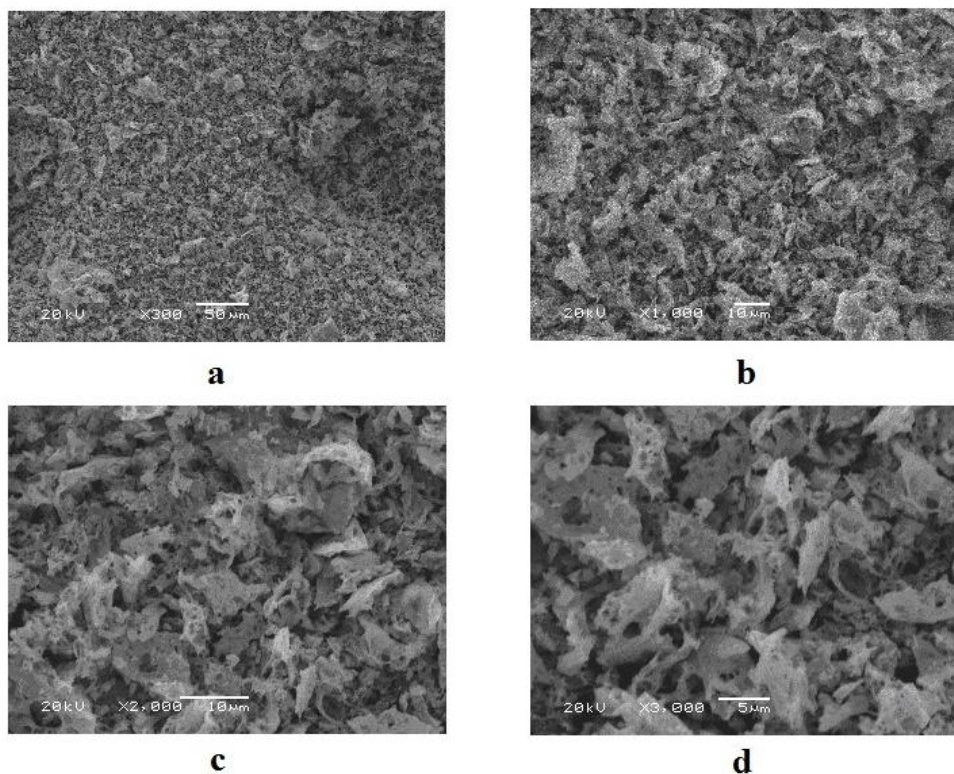

Figure 2. SEM images for $ZnFe_2O_4$ nano-particles with different magnifications.
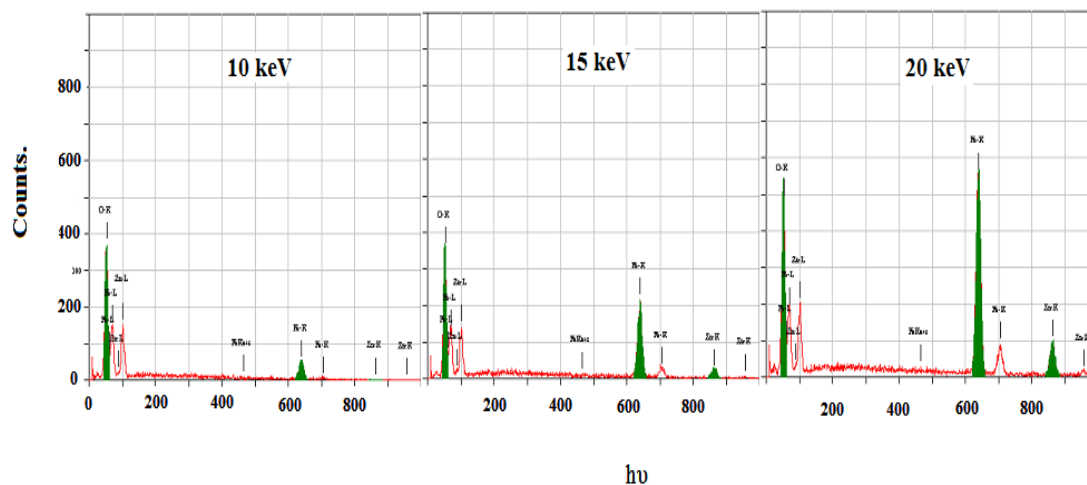
3.3. EDX analysis

Figure 3. EDX pattern of $ZnFe_2O_4$ nano-particles with different voltages.
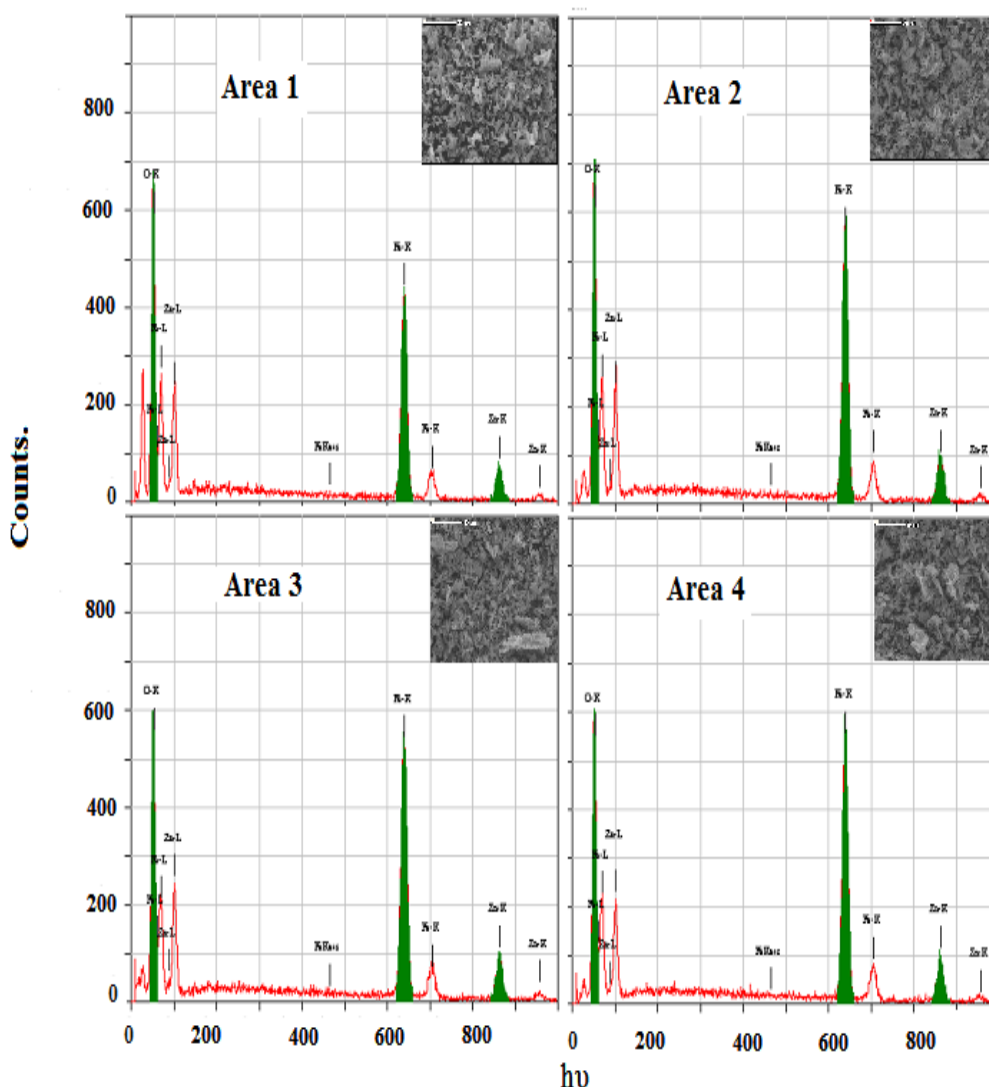
Figure 4. EDX pattern of $ZnFe_2O_4$ nano-particles with different areas.

Energy dispersive X-ray (EDX) analysis of the as prepared specimen was carried out at different voltages and various areas on the surface of solid. Figs. 3 and 4 display EDX analysis with different voltages and various areas, respectively. This finding shows almost homogeneous and uniform distribution of Zn and Fe particles in the powder sample.

The effective atomic concentration of Zn, Fe and oxygen species on top surface layers of the solid investigated are determined by EDX technique. The relative atomic abundance of Zn, Fe and O species present in the uppermost surface and bulk layers of Zn ferrite are given in Tables 1 and 2. Inspection of Table 1 revealed that the surface concentrations of Zn and Fe species at 10, 15 and 20 keV are very close to those in the bulk of the as synthesized solid. This observation may be reported to the increase in the mobility of Zn and Fe species with subsequent an increase in the formation of Zn ferrite. In addition, Table 2 showed that the surface concentrations of Zn, Fe and oxygen species at 20

keV on different areas over the surface of specimen studied are much closed to each other. This indicates the homogeneous distribution of Zn, Fe and O species in the investigated sample.

Table 1. The atomic abundance (surface and bulk) of elements measured at different voltages over the same area for the as prepared solids.

Elements	Atomic abundance (%)			
	Calculated (Bulk)	Found (Surface)		
		10 keV	15 keV	20 keV
O	26.55	22.37	22.50	22.50
Fe	46.33	77.73	54.90	54.89
Zn	27.12	00.00	23.60	23.61

Table 2. The atomic abundance (surface) of elements measured at 20 keV and different areas over the as prepared solids.

Elements	Area 1	Area 2	Area 3	Area 4
O	22.36	22.36	22.36	22.36
Fe	25.75	24.81	25.34	25.05
Zn	22.67	22.67	24.10	23.10

3.4. Magnetic properties

The saturation magnetization (M_S), remanent magnetization (M_r) and the coercivity of the as-prepared powders were determined by measuring the magnetic hysteresis loop (not given) at room temperature. The M_S value was found to be 60 emu/g and the value M_r was 20 emu/g for the $ZnFe_2O_4$ sample. The corresponding squareness ratio (M_r/M_s) was found to be 0.333. In addition, the coercivity of the investigated sample was found to 50 Oe. . It was found that the as-prepared Zn ferrite particles in this work exhibited a saturation magnetization greater than that of $ZnFe_2O_4$, prepared by glycine as fuel [32].

4. DISCUSSION

Spinel zinc ferrite, $ZnFe_2O_4$, based materials can be prepared via solid state reaction between ZnO and Fe_2O_3 [28]. The enhancement of this reaction is controlled by thermal diffusion of Zn and Fe cations through the zinc ferrite film which covers the surfaces of grains of reacting oxides (ZnO and Fe_2O_3) and acts as energy barrier. The precursor compounds, preparation method and preparation

conditions have different effects on solid state reaction between ferric and zinc oxides to produce Zn ferrite. In this study, the promoted combustion route was used for preparation of zinc ferrite. Indeed, the nature of fuel used in the combustion method affect the different properties of the as prepared ferrite such as structural, morphologically, surface, catalytic, optical and magnetic properties. In fact, the combustion process achieved by ammonium nitrate which produces from combination of nitrate and ammonium ions liberated from decomposition of the reactants [39]. So, the activation of the combustion route can be occurred by using a mixture of fuel and ammonium nitrate. This treatment resulted in reduction of local partial sintering among the primary particles via dissipation the heat of combustion reaction through the whole mass investigated [40, 41].

Formation of zinc ferrite nano-particles with moderate crystallization and low agglomeration can be achieved via the combustion route by using a mixture of glycine and ammonium nitrate depending upon the released heat and gases during the combustion process. So, the use of ammonium nitrate is promising route for formation of moderate crystalline zinc ferrite nano- particles due to distribution of the energy inside the whole reacting particles reducing the aggregation process as shown in SEM micrographs. Also, XRD measurement showed that Zn ferrite prepared by a mixture of glycine and ammonium nitrate has crystallinity less than that prepared by glycine only [32]

The counter-diffusion of Zn^{2+} and Fe^{3+} through a relatively rigid oxide lattice led to the formation of $ZnFe_2O_4$ particles [32]. Alper reported that the diffusing ions might be Fe^{2+} including Fe^{3+} on the basis of detecting Fe^{2+} in the interface [42]. In addition, following reactions indicate that Fe_2O_3 decomposes to $2Fe^{2+}$ and oxygen gas at Fe_2O_3–interface [43]. Moreover, oxygen moves through the reacted area to be added to the ZnO interface and form spinel by reacting with Fe^{2+} and ZnO:

At Fe_2O_3 interface:

$$3Fe_2O_3 + 2Zn^{2+} \quad \rightarrow \quad 2ZnFe_2O_4 + 2Fe^{2+} + 0.5O_2 \qquad (2)$$

At ZnO interface:

$$2Fe^{2+} + 3ZnO + 0.5O_2 \rightarrow \ ZnFe_2O_4 + 2Zn^{2+} \qquad (3)$$

The presence of any Fe^{3+} ions in ZnO by diffusion would contribute to the chemically created vacancies depending upon the ionic radii of ferric and zinc speices are 0.064 and 0.074 nm, respectively [32]. Indeed, $3Zn^{2+}$ could be replaced by $2Fe^{3+}$ and a vacancy because of electro-neutrality restrictions. However, ZnO–Fe_2O_3 system shows limited solid solution of Fe_2O_3 in ZnO solid. Ferric cations which appear in tetrahedral sites with the introduction of trivalent cations into ZnO can be considered as an embryonic element or nucleus for formation of inverse spinel in order to satisfy energy stabilization in the structure [44] .On the other hand, Fe^{3+} cations have a tendency to be located in tetrahedral sites with making a strong bond with O^{2-} ions in terms of electro-negativity differences and reach the lowest state of energy.

In this work, the observed super-paramagnetic behavior of Zn ferrite nano-particles could be attributed to spin canting and surface spin disorder that occurred in these nano-particles [45, 46].

Indeed, the zinc ferrite prepared by a mixture of glycine and ammonium nitrate has saturation magnetization (60 emu/g) greater than that for Zn ferrite synthesized by glycine only (52 emu/g) due to the redistribution of the reacting cations on A and B sites involved in the spinel Zn ferrite [32]. In other words, the higher saturation magnetization of Zn ferrite prepared in this investigation could be attributed migration of some Fe^{3+} ions from B site to A site via conversion of some Fe^{2+} ions to Fe^{3+} ions with subsequent increase in the Fe_A^{3+}–Fe_B^{3+} super-exchange interactions [47]. This conversion brought about an increase in the saturation magnetization and a decrease in the crystallinity of zinc ferrite prepared by using a mixture of glycine and ammonium nitrate comparing with that prepared by using glycine only. This decrease in the crystallinity could be attributed to the contraction in the lattice. This contraction may be due to the difference in the ionic radii of both ferric (0.076 nm) and ferrous ions (0.064) [32]. The saturation magnetization of the as prepared $ZnFe_2O_4$ nano-particles is clearly higher compared with the reported value of ~5 emu/g for the bulk $ZnFe_2O_4$ [23].

The large value of magnetization observed in the present study shows that the cation distribution changed from normal to mixed spinel type. Hence, the percentage of Fe^{3+} ions occupies the tetrahedral sites which switches on the A–B super-exchange interaction and gives rise in the magnetization. EXAFS studies conducted by Jeyadevan et al. support the presence of Zn^{2+} ion on the B-sites [48]. Liganza found that 4% of the A-sites was occupied by Fe^{3+} ions [49]. The neutron diffraction study of nanocrystalline $ZnFe_2O_4$ reports that the occupancy of Fe^{3+} ions at the A sites is 0.018 and 0.142 for the fine particles of diameters 96 and 29 nm, respectively [50]. However, it has been reported that the spin disorder may occur on the surface of the nano-particles and the cores of the nano-particles could be attributed to the vacant sub-lattice disorder sites (Fe_A^{3+}) and poor crystal structure [51].

5. CONCLUSIONS

Using a mixture of glycine and ammonium nitrate as fuel resulted in formation of Zn ferrite with moderate crystalline cubic spinel structure, homogeneously distributed nano- particles and nano-scale size. Higher saturation magnetization (60 emu/g) and coercivity values (50 Oe) of Zn ferrite are obtained by using a mixture of glycine and ammonium nitrate as fuel. These values are greater than those for nano-magnetic Zn ferrite materials prepared by using glycine only.

References

1. N. M. Deraz, S. Shaban, *J. Analyt. Appl. Pyrolysis*, 86 (2009) 173.
2. N. M. Deraz, M. K. El- Aiashy, Suzan. A. Ali, *Adsorp. Sci. Technol*. 27(2009)803.
3. N.M. Deraz, S.A. Shaban, A. Alarifi, *J. Saudi Chemical Society* 14(2010)357.

4. Y. KÖseoglu, A. Baykal, F. Gzüak, H. Kavas, *Polyhedron* 28 (2009) 2887.
5. Shao-Wen Cao, Ying-Jie Zhu, Guo-Feng Cheng, Yue-Hong Huang, *J. Hazard. Mater*. 171 (2009) 431.
6. Z.H. Zhou, J.M. Xue, J. Wang, H.S.O. Chan, T. Yu, Z.X. Shen, *J. Appl. Phys.* 91(2002) 6015.
7. Y. KÖseoglu, F. Yıldız, B. Aktas, G.S. Alvarez, M. Toprak, M. Muhammed, *Phys. Status Solidi* B 242 (2005) 1712.
8. M. Tsuji, Y. Wada, T. Yamamoto, T. Sano, Y. Tamaura, *J. Mater. Sci. Lett*. 15 (1996)156.
9. J.W. Choung, Z. Xu, J.A. Finch, *Ind. Eng. Chem. Res*. 38 (1999) 4689.
10. A.J. Rondinone, A.C.S. Samia, Z.J. Zhang, *J. Phys. Chem*. B (2000) 7919.
11. L.D. Tung, V. Kolesnichenko, G. Caruntu, D. Caruntu, Y. Remond, V.O. Golub, C.J. O'Connor, L. Spinu, *Physica* B 319 (2002) 116.
12. X. Chu, X. Liu, G. Meng, *Sens. Actuators* B 55 (1999) 12.
13. U. Steinike, K. Tkacova, *J. Mater. Synth. Process*. 8 (2000) 199.
14. S. Zhuykov, T. Ona, N. Yamazoe, N. Miura, *Solid State Ionics* 152–153 (2002) 801.
15. S.B. Li, G.X. Lu, *New J. Chem*. 16 (1992) 517.
16. G.X. Lu, S.B. Li, *Int. Hydrogen Energy* 17 (1992) 767.
17. Rahmatollah Rahimi, Hamed Kerdari, Mahboubeh Rabbani, Majid Shafiee*, Desalination* 280 (2011) 412.
18. S. Zhuiykov, M. Muta, T. Ono, M. Hasei, N. Yamazoe, N. Miura, *Electrochem. Solid-State Lett*. 4 (2001) H19.
19. S. Zhuiykov, T. Ono, N. Yamazoe, N. Miura, *Solid State Ionics* 152–153 (2002)801.
20. G. Zhang, L. Chunsheng, C. Fangyi, J. Chen, *Sensors & Actuators* B 120 (2007)403.
21. K. Arshak, I. Gaidan, *Mater. Sci. Eng*. B 118 (2005) 44.
22. J.Z. Zhang, D.H. Chen, L. Chen, *Sensors Mater*. 5 (2006) 227.
23. T.M. Clark, B.J. Evans, *IEEE Trans. Mag*. 33 (1997) 3745.
24. J.L. Mart´ın de Vidales, A. L´opez-Delgado, E. Vila, F.A. L´opez, *J. Alloys Compd*. 287 (1999) 276.
25. S.H. Yu, T. Fujino, M. Yoshimura, *J. Magn. Magn. Mater*. 256 (2003)420.
26. J.A. Toledo, M.A. Valenzuela, P. Bosch, H. Armendáriz, A. Montoya, N. Nava, A. V´azquez, *Appl. Catal*. A 198 (2000) 94.
27. N.S. Gajbhiye, U. Bhattacharya, V.S. Darshane, *Thermochim. Acta* 264 (1995) 219.
28. C. N. Chinnasamy, A. Narayanasamy, N. Ponpandian, K. Chattopadhyay, H. Guerault, J. M. Greneche, *J. Phys.Condens. Matter*. 12 (2000) 7795.
29. C. N. Chinnasamy, A. Narayanasamy, N. Ponpandian, K. Chattopadhyay, H. Guerault, J. M. Greneche, *Scripta Mater*. 44 (2001) 1407.
30. L. Néel, Comput. Rend. 252 (1961) 4075.
31. N. M. Deraz, A. Alarifi, *Int. J. Electrochem. Sci*., 7 (2012) 3798.
32. N. M. Deraz, A. Alarifi, *Polyhedron*, 28(2009) 4122.
33. N. M. Deraz, A. Alarifi, *Int. J. Electrochem. Sci*., 7 (2012) 3809.
34. N. M. Deraz, *J. Analyt. Appl. Pyrolysis*, 91(2011) 48.
35. T. Sato, K. Haneda, M. Seki, T. Iijima, *Appl. Phys*. A 50 (1990) 13.
36. P.B. Avakyan, E.L. Nersisyan, M.D. Nersesyan, *Int. J. SHS*. 4(1995) 79.
37. Y. Li, J.P. Zhao, J.C. Han, *Mater. Res. Bull*. 37(2002) 583.
38. B.D. Cullity, Elements of X-ray Diffraction, Addison-Wesly Publishing Co. Inc. 1976 (Chapter 14).
39. P. Priyadharsini, A. Pradeep, G. Chandrasekaran, *J. Magn Magn. M*ater. 321(2009)1898.
40. N. M. Deraz, *Current Applied Physics* 12 (2012) 928.
41. N. M. Deraz, *Int. J. Electrochem. Sci*., 7 (2012) 4608.
42. Alper, High Temperature Oxides, Academic Press, New York, 1970.
43. A. Azhari, M. Sharif Sh., F. Golestanifard, A. Saberi, *Mater. Chem. Physics* 124 (2010) 658.

44. S.L. Blank, J.A. Pask, *J. Am. Ceram. Soc.* 52 (1969) 669.
45. Z. Gu, X. Xiang, G. Fan, F. Li, *J. Phys. Chem*. C 112 (2008) 18459.
46. L. Ai, J. Jiang, *Curr. Appl. Phys*. 10 (2010) 284.
47. L. Jianjun, Y. Hongming, L. Guodong, L. Yanju, L. Jinsong, *J. Magn. Magn. Mater*. 322(2010)3396.
48. B. Jeyadevan, K. Tohj, K. Nakatsuka, *J. Appl. Phys.* 76 (1994) 6325.
49. S. Liganza, *Phys. Stat. Sol*. 75 (1976) 315.
50. F.K. Lotzering, *J. Phys. Chem. Solids* 27 (1996) 139.
51. M. P. Morales, S. Veintemillas-Verdaguer, M. I. Montero, C. J. Serna, A. Roig, L. Casas, B. Martînez, F. Sandiumenge, *Chem. Mater*. 11(1999)3058.